Preferential dissolution of copper from Cu-Mn oxides in strong acid medium: Effect of the starting binary oxide to get new efficient copper doped MnO2 catalysts in toluene oxidation

Zhiping Ye, Jean-Marc Giraudon, Nicolas Nuns, Grêce Abdallah, Ahmed Addad, Rino Morent, Nathalie de Geyter, Jean-François Lamonier

Preferential dissolution of copper from Cu-Mn oxides in strong acid medium: effect of the starting binary oxide to get new efficient copper doped MnO_2 catalysts in toluene oxidation

Zhiping Ye[a,d], Jean-Marc Giraudon[a*], Nicolas Nuns[b], Grêce Abdallah[a,d], Ahmed Addad[c], Rino Morent[d], Nathalie De Geyter[d], Jean-François Lamonier[a]

[a]*Univ. Lille, CNRS, Centrale Lille, Univ. Artois, UMR 8181 - UCCS - Unité de Catalyse et Chimie du Solide, Lille, 59000, France*

[b] *Univ. Lille, CNRS, Centrale Lille, Univ. Artois, IMEC-Institut Michel-Eugène Chevreul, Lille, 59000, France*

[c]*Univ. Lille, CNRS, UMR 8207 – UMET, Lille, F-59000, France*

[d]*Ghent University, Faculty of Engineering and Architecture, Department of Applied Physics, Research Unit Plasma Technology, Sint-Pietersnieuwstraat 41 B4, 9000 Ghent, Belgium*

**Corresponding author: jean-marc.giraudon @univ-lille.fr*

Abstract: This work investigated the concept of preferential dissolution of copper in HNO_3 10M at 20 °C from two starting Cu-Mn oxides to acquire novel copper doped MnO_2 like polymorphs. On purpose two starting Cu-Mn oxides were tested: a nanocristalline $CuMn_2O_4$ spinel phase with a SSA of 47 m^2/g and a weak amorphous Cu-Mn oxide with a Mn/Cu atomic ratio of 4.8 (SSA: 166 m^2/g). The physico-chemical properties of the final copper doped MnO_2 like oxides were discussed in terms of the nature of the starting oxides and of the operating conditions applied for the acid treatment. Finally, these new copper doped γ/ε MnO_2 like oxides were assessed in toluene oxidation and their catalytic performances were compared with those of α-MnO_2 and ε-MnO_2 catalysts. The copper doped MnO_2 obtained from the weak amorphous Cu-Mn oxide exhibited the highest activity in terms of $T_{50}(CO_2)$. This highest activity was related to a high density of Cu-O-Mn interactions at the outermost layers of the catalyst as assessed by ToF-SIMS results.

Keywords: Preferential dissolution, Acid treatment, ε/γ -MnO_2, Toluene, Total oxidation catalysis, Cu-Mn mixed oxides

1. Introduction

MnO_2 has attracted a growing attention among transition metal oxides (TMO) for total catalytic oxidation due to its attractive redox chemistry, non-stoichiometric composition, low cost and environmental compatibility. Various polymorphs of MnO_2 exist differentiating by the three-dimensional packing of MnO_6 octahedra units. Among the different strategies of MnO_2 preparation very little work has been reported on the cation selective dissolution in acid media starting from Mn based binary oxides apart those from normal spinel AMn_2O_4 compounds (A = Li) [1] and very recently those from $LaMnO_3$ [2,3]. Aqueous acid treatment of $LiMn_2O_4$ at ambient resulted in the formation of λ-MnO_2 in which the spinel structure was preserved with most of the lithium removed from the tetrahedral sites. In a similar way it was reported that the treatment in diluted HNO_3 of a three-dimensionally ordered macroporous $LaMnO_3$ perovskite selectively removed La cations to get a novel γ-MnO_2-like material exhibiting improved catalytic properties in CO oxidation [2] and in total oxidation of toluene [3]. In this type of "acid mediated synthesis" a residual amount of the leached cation (Li^+, La^{3+}) was always observed.

Consequently, acid treatment performed on starting mixed oxides containing two transition metals (TM) offers *a priori* an easy way of achieving efficient doping of MnO_2 polymorphs [4,5]. Among TM cations, copper cation seems to be one of the most suitable candidates for cationic doping because of its low cost, good electrical conductivity and environmentally benign nature and good performances in total oxidation of volatile organic compounds (VOC). On purpose, R. Kumar et al. have previously investigated the effect of the physicochemical characteristics of Ni and Cu containing birnessites on the leachability of the TM elements in sulfuric acid [6,7]. Anomalous dependence of leachability on surface area during sulfuric acid leaching of Cu containing birnessite was explained in terms of transformation of the birnessite into a more compact structure, γ-MnO_2, with a fraction of Cu which remained unleached.

Generally speaking, acid treatment conditions (nature and concentration of the acid, duration, temperature) and nature of the starting binary oxides are recognized to be key parameters for the "acid mediated synthesis" of MnO_2 like polymorphs.

In this work the possibility to extent the concept of selective dissolution in acidic medium to acquire novel copper doped MnO_2-like polymorphs was explored using two bulk copper manganese oxides as starting oxide materials. These oxide materials differ from their Cu/Mn stoichiometry, structure, extent of crystallinity, specific surface area (SSA) and redox properties (different Mn average oxidation state (Mn AOS)).

The first structure is a well crystallized $CuMn_2O_4$ spinel phase with a SSA of 47 m^2/g synthesized by-coprecipitation [8] using tetramethylammonium hydroxide (TMAH) as precipitating agent. The bulk Mn AOS of 3.2, slightly higher than 3.0, is due to the simultaneous detection of the Cu^{2+}/Cu^{+} and Mn^{4+}/Mn^{3+} valences at the oxide surface by XPS likely resulting from the redox process: $Cu^{2+} + Mn^{4+} = Cu^{+} + Mn^{3+}$. Additionally, H. Einaga et al. have shown from Mn and Cu K-edge EXAFS curve-fitting results that Cu and Mn ions were located both in octahedral and tetrahedral sites of the Cu-Mn spinel phase [8]. The second precursor is a weak amorphous Cu-Mn oxide synthesized by a redox-precipitation method [9] followed by a calcination at 300 °C for 2 h. This type of material has been previously ascribed to a copper containing layered-type MnO_2 birnessite having a turbostratically disordered structure [10-12]. This resulting Cu-Mn oxide exhibits a Cu/Mn atomic ratio of 0.21, a SSA of 166 m^2/g and a Mn AOS of 3.8 [13].

In this work the effect of an HNO_3 10M treatment at room temperature over the two Cu-Mn oxides has been for the first time investigated through the transformation of the starting materials into Cu-doped MnO_2 materials. The catalytic performances of these new calcined acid treated catalysts have been assessed in total oxidation of toluene to be compared with those of α-MnO_2 and ε-MnO_2 catalysts resulting from acid-treatment of amorphous birnessite like-MnO_2 and $LaMnO_3$, respectively. The catalytic performances of the acid-treated catalysts have been discussed considering their physico-chemical properties.

2. Experimental

2.1. Preparation of the catalysts

The spinel-type $CuMn_2O_4$ (CuMn-S) was prepared using a co-precipitation method as already reported [8]. The weak amorphous Cu-Mn oxide (CuMn-B) was prepared using the redox-precipitation method [9]. The acid treatment was typically performed by immersing 500 mg of Cu-Mn oxide powder in 50 mL of an aqueous solution of HNO_3 10M (Aesar; 65-70 %). The reaction was carried out at 20 °C under stirring with a magnetic stirrer (350 rpm) for 65 h (CuMn-S) and 5 h (CuMn-B). The final suspension was filtered, washed with distilled water until pH was that of distilled water and dried overnight at 100 °C. The resulting powders were calcined at 300 °C for 2 h. The final samples were labelled AT-CuMn-S and AT-CuMn-B (AT: acid treated). The suffixes WW and NC were added for the acid-treated catalysts without subsequent washing and for the non-calcined catalysts, respectively.

For sake of comparison a weak amorphous manganese oxide (AMO) disordered polymorph Mn-B sample was synthesized via the redox method followed by a calcination step at 300 °C for 2 h [13]. The acid-treatment was similar as that performed for CuMn-B and the resulting sample was labelled AT-Mn-B. A reference ε-MnO_2 (AT-LaMn-P) was obtained through a 10M HNO_3 treatment of a rhombohedral $LaMnO_{3+\delta}$ (LaMn-P) perovskite synthesized owing to the citrate method following the same experimental procedure given elsewhere [14] for 15 h in the same conditions as above followed by a subsequent calcination at 300°C for 2 h. Here, the S, B and P coding stands for spinel, birnessite and perovskite, respectively.

2.2. Catalyst characterization

The phase and crystal structure of the products were analyzed by X-ray diffraction (XRD) using a X-ray diffractometer Bruker AXS D8 Advance with Cu-Kα radiation (1.5418 Å).

The morphology and microstructure of the as-synthesized samples were characterized by scanning emission spectroscopy (SEM, JSM-7800F) equipped with an energy dispersive spectrometer (EDS) used for semi-quantititative TM quantification.

Cu/Mn atomic ratio was also determined from elemental analyses performed with an inductively coupled plasma-optic emission spectroscopy 720-ES ICP-OES (Agilent) spectrometer with axially viewing and simultaneous CCD detection. The sample preparation was made by dissolving 10 mg of dried and ground samples in concentrated aqua regia solution (HNO_3:HCl) (1:3, v:v). After heating up to 110°C in a Vulcan autodigestor for 2 h, the resulting solution was diluted up to 20 ml by ultrapure water before being analyzed by ICP-OES.

Transmission electron microscopy characterization was performed using a TECNAI TEM operating at an accelerating voltage of 200 kV. The prepared powders were deposited onto a carbon-coated copper grid for TEM observation.

The thermogravimetric analysis and the differential scanning calorimetry and (TGA/DSC) were performed in air atmosphere on a SDT Q600 V20.9 Build 20 instrument. The temperature range was from 25 °C to 1,000 °C with a heating rate of 10 °C/min.

The specific surface area was determined by BET method with nitrogen adsorption-desorption at -196 °C using a Quantachrome Quadrasorb SI analyser. Prior to the measurements, the samples were degassed at 300 °C for 5 h.

Temperature programmed reductions (TPR) were carried out on about 50 mg of the sample under 5 vol% H_2/Ar gas flow (50 mL/min) with a heating rate of 5 °C/min up to 500 °C using a Micromeritics Autochem II 2920 apparatus.

ToF-SIMS data were acquired using a ToF-SIMS5 spectrometer (ION-TOF GmbH Germany) equipped with a bismuth liquid metal ion gun (LMIG). The powders were crushed using an agate mortar and pestle and the standard tablets were prepared using a press machine. The samples were bombarded with pulsed Bi_3^+ primary ion beam (25 keV, 0.25 pA) rastered over a 500 µm × 500 µm surface area. With a data acquisition of 70 s, the total fluence did not amount up to 10^{12} ions/cm^2 ensuring static conditions. Charge effects were compensated by means of a 20 eV pulsed electron flood gun. Under these experimental conditions, the mass resolution (m/Δm) was about 6000 at m/z 55 for Mn^+. Data were collected over a mass range m/z = 0-800 for both positive and negative secondary ions. The fragments were identified by their exact mass, coupled with the appropriate intensities for the expected isotope pattern. The use of isotopic patterns for the copper (^{63}Cu and ^{65}Cu with abundance of 69.15% and 30.85%, respectively) and for Mn (^{55}Mn with abundance of 100 %) reinforced the ion assignment.

XPS experiments were performed using an AXIS Ultra DLD Kratos spectrometer equipped with a monochromatized aluminum source (Al K_α = 1486.7 eV) and charge compensation gun. Adventitious carbon contamination was used as a charge reference for XPS spectra and all binding energies (BE) were referenced by setting the C-C/C-H component to a binding energy (BE) of 284.8 eV. The XPS photopeaks with multiple components were resolved by a peak-fitting program assuming a mixed Gaussian (70%)/Lorentzian (30%) peak shape using the software supplied by CasaXPS. Semi-quantitative analysis accounted for a Shirley background subtraction. The Mn $2p_{3/2}$ peak was fitted with 6 peaks of equal FWHM characteristic of MnO_2 according to the procedure of Biesinger et al. [15]. The Mn AOS was determined by XPS from the linear correlation between the energy separation (E) of the two Mn 3s components and the Mn AOS, namely Mn AOS = 8.956 – 1.13E, given by Santos et al. [16].

Catalytic oxidation runs for abatement of toluene were performed in a continuous flow fixed bed Pyrex micro-reactor at atmospheric pressure. About 0.2 g of catalyst was placed in the reactor (1 cm in internal diameter) for each run. To obtain accurate and stable gas flow rates, mass flow controllers were used. The concentration of toluene was 800 ppmv, which was controlled by the temperature of a home-made saturator and the additional airstream. The flow rate of the gas mixture through the reactor was 100 mL/min, which gave a Gas Hourly Space Velocity (GHSV) of 30 L/(g.h). The micro-reactor was placed in an electrical furnace providing the required temperature for catalytic reaction. Catalysts performances were evaluated by decreasing the temperature from 300 °C to 25 °C, with a decreasing rate of 0.5 °C/min. Before each run, the samples were pretreated for 2 h at the temperature of calcination in flowing air (75 mL/min). The concentrations of the inlet and outlet gas stream were analyzed online by Gas Chromatography

(7860A Agilent Gas Chromatograph) equipped with a Thermal Conductivity Detector (TCD) and Flame Ionization Detector (FID) and with two columns: RestekShin Carbon ST/Silco HP NOC 80/100 micropacked, to separate permanent gases (Air, CO and CO_2) and a capillary column Cp-Wax52 CB25 m, Ø ¼ 0.25 mm, to separate hydrocarbons and aromatic compounds. Toluene conversion (Ct) into CO_2 was calculated as follows: Ct (%) = $[CO_2]_{out}/7[toluene]_{in}$ where $[toluene]_{in}$ was the concentration introduced in the reactor and $[CO_2]_{out}$ was the CO_2 concentration in the off gas.

A stability test was performed on the Cu-Mn acid-treated catalysts. Prior to the stability test, the catalyst was treated in air (75 mL/min) at the temperature of calcination for 2 h (10 °C/min). The catalyst was subsequently submitted to 1000 ppm of toluene diluted in air (O_2 = 21 %, N_2 balance, GHSV = 30 L/(g_{cat}.h) at 240 °C, and the evolution of toluene conversion was monitored for 9 h.

3. Results and discussion

3.1. *Acid treatment over the Cu-Mn oxides*

The acidic treatment has been conducted in HNO_3 10M over the Cu-Mn oxides at 20 °C. For both starting suspensions, the acidic solution turns progressively green in the course of the reaction in accordance with the release of copper via Cu(II) nitrato complexes. The extent of $CuMn_2O_4$ dissolution has been quantified from the weight of the calcined sample. It is found that the weight loss (in wt%) increases from 45.4 to 58.9 when increasing the acid treatment duration from 5 h to 65 h (Table **1**). Based on the disproportionation of Mn^{3+} in the starting oxide solid, the complete transformation of $CuMn_2O_4$ into MnO_2 assuming a total release of Cu^{2+} and Mn^{2+} in solution occurs owing to the formal reaction:

$$CuMn_2O_4 + 4H^+ = MnO_2 + Cu^{2+} + Mn^{2+} + 2H_2O$$

Consequently, the relative weight losses given above result in phase transformation yields of 71 % and 93 % for durations of 5 h to 65 h, respectively.

Table 1. Weight loss after acid-treatment (AT)

	AT duration /h	weight loss /%
CuMn-S	5	45.4 (71[a])
	65	58.9 (93)
CuMn-B	5	20.0

a: phase transformation yield.

In contrast to the spinel phase, the weight loss for CuMn-B after 5 h of 20.0 wt% is about two time less than the value for CuMn-S. This result is consistent with the high Mn^{4+} content (bulk Mn AOS of 3.8) [13] in this sample precluding release of substantial amount of Mn^{2+} throughout the dismutation of Mn^{3+}.

The Cu/Mn atomic ratios in the acid treated solids are significantly lower than those in the initial oxide reactants (Table **2**) indicating that most of Cu^{2+} is released into the solution under highly acidic conditions. It should be noted that the relative amount of Cu^{2+} released into the solution is higher for the starting birnessite as compared to the spinel sample after 5 h of acid treatment as the Cu/Mn atomic ratio decreases by a factor of about 10 and 2 for CuMn-B and CuMn-S, respectively. The differences in terms of Mn^{3+} content, Cu^{2+} environment and degree of crystallinity between the two starting Cu-Mn oxides may explained such a result. Additionally, the Cu/Mn atomic ratio of 0.56 for CuMn-S decreases with time to reach 0.27 after 5 h and 0.037 after 65 h of acid treatment, respectively.

Table 2. Physico-chemical properties of the catalysts

	Cu/Mn[a]	K/Mn	SSA / $m^2.g^{-1}$	V /$cm^3.g^{-1}$	H_2 consumption / $mmol.g^{-1}$
CuMn-S	0.56	-	48	0.30	-
AT-CuMn-S	0.078 (0.037[b])	-	91	0.40	10.55
CuMn-B	0.21	-	166	0.30	-
AT-CuMn-B	0.019 (0.29[b])	-	105	0.37	10.63
Mn-B	-	0.103	384	0.66	-
AT-Mn-B	-	0.019	168	0.44	8.59
AT-LaMn-P	-	-	85	0.33	10.41

a: molar ratio (EDX); b: from ICP-OES

It is worthy to note that a significant fraction of copper remains unleached, even after prolonged acid-treatment. These results can be interpreted in terms of structural changes during leaching as previously observed [7].

3.2. Structural, textural and morphology characterization (XRD, N_2-sorption, SEM)

Fig. **1** shows the X-ray diffraction patterns at the different steps of the acid treatment performed on CuMn-S. The diffraction peaks of the starting $CuMn_2O_4$ are well indexed to the face-centered-cubic (fcc) $CuMn_2O_4$ (JCPDS No. 01-076-2296, space group: Fd-3m, a = 8.33 Å) with a spinel structure. The X-ray diffraction pattern of the recovered powder after acid treatment of 65 h duration (Fig. **1a**) exhibit new peaks well indexed to a mixture of two polymorphs of MnO_2, namely λ-MnO_2 (JCPDS No. 00-044-0992) and γ-MnO_2 (JCPDS No. 00-014-0644). Additionally, the relative content of γ-MnO_2 increases after washing (Fig. **1b**) to be the

predominant detected crystallized phase after calcination (Fig. **1c**). These observations suggest that the phase transformation of $CuMn_2O_4$ into γ-MnO_2 proceeds through the spinel λ-MnO_2 phase as an intermediate species which progressively converted into γ-MnO_2 in the presence of water. Such a phase transformation can occur through a dissolution-crystallization mechanism as previously reported by Larcher et al. for the transformation of the delithiated λ-MnO_2 into γ-MnO_2 prepared from the digestion of $LiMn_2O_4$ [17]. Noteworthy, the X-ray diffraction pattern of the unwashed sample sometimes shows two additional narrow peaks (not shown here) located at 12.80 ° and 25.77 ° in 2θ which are consistent with a dicopper trihydroxide nitrate as rouaite (JCPDS No. 015-4100) and/or gerhardtite phase [18]. These minerals are well known to be corrosion compounds of copper with HNO_3. However, these products are released from the surface of the material after extensive aqueous washing.

The X-ray diffraction pattern of the starting oxide CuMn-B (Fig. **2a**) shows two broad diffraction peaks located at 2θ = 37.2º and 65.7 ° whose positions agree with those of turbostratic hexagonal birnessite reported in the literature [10-12]. The peak broadenings indicate a very low crystallinity of the sample. The X-ray diffraction patterns recorded after acid treatment (Fig. **2b**) of 5 h duration shows 4 new peaks located at 37.3, 42.5, 56.5 and 66.2° and a large peak at about 22 ° relative to ε-MnO_2 [19]. However, after calcination at 400 °C all X-ray diffraction peaks shift to higher angles and significantly broaden. These observations already observed in the literature were related to an increase of the relative concentration of pyrolusite micro-domains in the MnO_2 matrix during heating [20].

The X-ray diffraction pattern of the starting oxide Mn-B is similar to that relative to CuMn-B consistent with a hexagonal turbostratic birnessite (Fig. **S1**). All the diffraction peaks of the final product after acid treatment and subsequent calcination (300 °C for 2 h) have been indexed to cryptomelane (α-MnO_2, JCPDS No. 044-0141). The high K^+ content in the starting material allows to maintain a K/Mn ratio of 0.19 after acid treatment allowing the formation of one dimensional (0.46 × 0.46 nm) tunnels formed by corner and edge sharing manganese octahedral [MnO_6] units where charge neutrality is maintained by K^+ residing in the tunnels. As shown in Fig. **S2** the X-ray diffraction pattern of AT-LaMn-P does not anymore display the relevant peaks of the rhombohedral $LaMnO_{3+\delta}$ perovskite phase but those characteristics of **ε**-MnO_2. This result differs slightly from those of Si et al. [2] who reported the formation of γ-MnO_2 through acid treatment of $LaMnO_{3+\delta}$ but with different experimental conditions.

Fig. **S3** displays the N_2 adsorption/desorption isotherms and the corresponding pore size distribution curves for the different materials. A typical type IV isotherm was observed for the

Cu containing MnO_2 samples with a hysteresis loop indicating the existence of a mesoporous structure (Fig. **S3a**) with a broad pore size distribution for AT-CuMn-S (Fig. **S3b**). Despite the differences of the textural properties observed for the two starting Cu-Mn oxides, the resulting MnO_2 show rather similar textural properties in terms of SSA and pore volume. Indeed, the SSA for AT-CuMn-S and AT-CuMn-B were 91 and 105 m^2g^{-1}, and the corresponding pore volumes were 0.40 and 0.37 cm^3g^{-1}, respectively. Additionally, the important change in surface area whatever the starting materials provides a good indication of structural rearrangement during doping [4]. For the free copper acid treated samples the same type of isotherms is observed (Fig. **S3c**) and a narrow pore size distribution is observed for AT-Mn-B (Fig. **S3d**).

The morphologies of the as-prepared and acid treated copper manganese oxide samples have been investigated by SEM observation (Fig. **S4**). The particles are irregular and random in shape for the two starting oxides. Acid treatment results in additional formation of small particles from larger ones.

3.3 Selected area electron diffraction characterization

The structure of the acid-treated Cu-Mn oxides as well as that of AT-LaMn-P was further investigated by selected area electron diffraction (SAED) and TEM (Fig. **S5**). The bright spots on concentric circles in the SAED pattern show the monocrystalline nature of the oxide particles for the three samples. The SAED pattern of AT-CuMn-S shows characteristic diffraction rings ascribed to the (100), (230), (300), (002), (160) and (420) planes of the orthorhombic phase of γ-MnO_2 without excluding the presence of some residual ε-MnO_2, α-MnO_2 and Mn_2O_3. By opposition, the SAED pattern of AT-CuMn-B and AT-LaMn-P exhibit four diffraction rings, corresponding to the (100), (10l), (102) and (110) planes of ε-MnO_2. TEM images of AT-CuMn-S and AT-CuMn-B show oblong nanoparticles while those of AT-LaMn-P show agglomerated bundles of rod like particles.

3.4. TG/DSC Analysis

TG/DTG curves and DSC profiles for the two Cu-Mn acid treated solids, calcined or not, performed in dry air are displayed in Fig. **S6** and the relevant results are given in Table **S1**. The TG curves of the two non-calcined catalysts show a total weight loss of 13.34 and 18.51 wt% for the AT-CuMn-S-NC and AT-CuMn-B-NC precursors, respectively. Based on the DTG curves, the calcination appears to be a complex multi-step process. To sum up, three significant weight loss steps can be identified for both samples. The weight loss from 20°C up to 380°C is due to the release of physisorbed water (20 °C-100 °C) and chemically bonded water (100 °C-400 °C).

This chemically bonded water in the form of OH ions has been related to either Mn^{4+} vacancies and Mn^{3+} in the network of MnO_2. The second weight loss (400 °C-600 °C) for which the DSC (Differential Scanning Calorimetry) curve exhibits two endothermic peaks can be attributed to the formation of Mn_5O_8 and Mn_2O_3. Increasing further the temperature may lead to a weight loss related with the endothermic transformation of Mn_2O_3 into Mn_3O_4.

The differential thermogravimetric (DTG) curves of the two calcined samples have similar behavior showing three separate steps in the temperature range of 25 °C-990 °C. The first step consists of the release of physisorbed water up to 110°C followed by that of chemisorbed water up to 400°C. The second and third weight loss steps consist of the successive phase transformations: MnO_2 into Mn_2O_3 and Mn_2O_3 into Mn_3O_4 consistent with the observance of the associated endothermic peaks (Fig. **S6d**). The thermal process related to the phase transformation of MnO_2 into Mn_2O_3 accompanied with the depletion of oxygen appears about 20 °C lower for AT-CuMn-B in comparison to AT-CuMn-S. Consequently, as the textural properties and crystal structures of the two materials are rather similar, improvement of the mobility and availability of the lattice oxygen for AT-CuMn-B can be explained by an increase of the dopant content.

3.5. Reducibility studies

Fig. **S7** illustrates the H_2-TPR profiles of the acid treated samples, and the results are listed in Table **1**. The H_2-consumption traces are very similar for both samples. It is found two main reduction peaks positioned at 244 °C (247) and 268 °C (263) preceded by a shoulder at about 195-200 °C corresponding to a total H_2 consumption of 10.63 and 10.55 mmol/g for AT-CuMn-B and AT-CuMn-S, respectively. These amounts are in line with that of 10.68 mmol/g found for the theoretical transformation of γ-MnO_2 into MnO [3]. This is consistent with the total reduction of remaining Cu^{2+} into Cu^0 and that of MnO_2 into MnO. Interestingly Cu^0 can assist the reduction of the Mn species at low temperature by hydrogen spill-over. The Mn AOS increases from 3.2 to 4.0 and from 3.8 to 4.0 after acid treatment for CuMn-S and CuMn-B, respectively. This increase is consistent with the expected disproportionation reaction of Mn^{3+}(s) to give MnO_2(s) and Mn^{2+}(aq). A direct comparison with the H_2-TPR envelopes of AT-LaMn-P and AT-Mn-B shows that the presence of copper promotes significantly the reducibility of the material in terms of decreasing the onset reduction temperature and reducing the temperature range of the reduction process.

3.6. Surface characterization (XPS and ToF-SIMS)

The XPS data as well as the XPS Cu 2p core level spectra of the 2 starting Cu-Mn oxides at each step of the process are given in Table **S2** and in Fig. **S8**. Regarding CuMn-S, the Cu $2p_{3/2}$ core level for the spinel sample shows two separate peaks at 931.2 eV and 934 eV ascribed to the coexistence of Cu(I) and Cu (II) in octahedral and tetrahedral sites [13]. After acid treatment it is observed a strong decrease of the Cu(I) component which practically disappears after calcination while the Cu(II) component appears as a broad low intensity peak. Conversely only one component ascribed to Cu(II) is observed for CuMn-B at 934.3 eV [13]. This Cu component likewise decreases strongly in intensity and broadens after acid treatment and such a decrease is accentuated after calcination. Anyhow the Cu $2p_{3/2}$ peak is located at 933.9 eV in both samples. Overlapping of the Mn Auger peak with the Cu $2p_{3/2}$ envelope does not allow to quantify the Cu amount. Anyway, the presence of a distinct Cu 3p contribution close to that of Mn 3s for AT-CuMn-B which is not observed for AT-CuMn-S indicates a surface copper enrichment for the acid-treated birnessite-like sample. The Mn $2p_{3/2}$ core level envelope for the two starting Cu-Mn oxides and acid treated samples has been simulated successfully by the co-existence of Mn^{3+} and Mn^{4+} according to the procedure of Biesinger et al.[13] and the simulated Mn $2p_{3/2}$ XPS spectra regarding CuMn-S before and after acid-treatment and calcination are shown in Fig. **S9**. This leads to estimated Mn AOS of 3.7 for the two starting Cu-Mn oxides to increase to 3.9 and 3.8 for AT-CuMn-S and AT-CuMn-B, respectively.

Additionally, the Mn AOS has also been estimated from the BE separation of the 2 split components of Mn 3s [16]. From Table **S2**, the Mn AOS values are estimated in the 3.5-3.7 range considering all steps of the process irrespective of the catalyst. These values are slightly less than those obtained from the Mn 2p core level

The O 1s spectra can be decomposed into four peaks (not shown here). The intense peak at around 529.7 eV is assigned to surface lattice oxygen O^{2-} (denoted as O_{lat}) while the peak at higher BE of 533.5 eV is ascribed to adsorbed water [13]. Two other O 1s components at 532.2 eV and 531.1 eV have been ascribed to adsorbed oxygen species (O_{ads}). The atomic $O_{ads}/(O_{ads} + O_{lat})$ ratios are 0.36 and 0.40 for AT-CuMn-S and AT-CuMn-B, respectively. The higher relative contribution of surface adsorbed oxygen species for AT-CuMn-B is consistent with the higher substitutional doping of Cu cations into the γ-MnO_2 framework.

The outermost surface of the Cu-Mn oxides has also been probed by ToF-SIMS at each step of the processing. Indeed, the molecular specificity and surface sensitivity of ToF-SIMS have been shown to be extremely useful in the surface characterization (depth of about 3-4 nm) of heterogeneous catalysts [21]. From Table **3**, it is noted a 8-fold and 6-fold decrease of the ToF-SIMS secondary ion intensity ratio, Cu^+/Mn^+, after HNO_3 10M treatment for CuMn-S and

CuMn-B, respectively. These results are fully consistent with the high leachability of Cu as compared to Mn in 10M HNO_3 medium. By contrast this intensity secondary ion Cu^+/Mn^+ ratio remains constant after calcination for CuMn-B suggesting that this subsequent step does not affect so much the relative TM distribution at the outermost layers of the catalyst. Interestingly, the ToF-SIMS spectra of the acid treated samples always exhibit a series of $Cu_xMn_yO_zH_w^{\pm}$ secondary ions which are considered as the fingerprint of the formation of a mixed oxide [13, 22,23].

Table 3. ToF-SIMS characterizations of the different catalysts

Catalysts	Cu^+/Mn^+	$MnOCu^+/Cu^+$
CuMn-S	0.16	0.36
AT-CuMn-S-NC	0.02	0.24
AT-CuMn-S	-	0.28
CuMn-B	0.12	0.26
AT-CuMn-B-NC	0.02	0.26
AT-CuMn-B	0.02	0.36

The ToF-SIMS spectra in polarity (+) in the m/z range 133.5-137 of CuMn-S and AT- CuMn-S given in Fig. **3** show the secondary ions $CuMnO^+$ and $CuMnOH^+$ and the related isotopic $^{65}CuMnO^+$ and $^{65}CuMnOH^+$. This indicates that a strong interaction is preserved between manganese and remaining copper after acid treatment and this holds also for CuMn-B. Besides, the ToF-SIMS intensity secondary ion $MnOCu^+/Cu^+$ ratio of 0.25 ± 0.01 is similar for both samples after acid treatment. However, on contrary to the acid-treated spinel oxide, it is found for AT-CuMn-B a significant enhancement of the $MnOCu^+/Cu^+$ intensity ratio after calcination which increases from 0.26 to 0.36 indicating the beneficial role of the calcination step in promoting the Mn-O-Cu interactions.

3.7. Catalytic oxidation of toluene

Fig. **4** shows the light-off curves of the catalysts in the total oxidation of toluene. $T_{50(CO2)}$ (the reaction temperature corresponding to 50% of the toluene conversion into CO_2) has been used to compare the catalytic activities of the samples. The catalysts can be ranked by decreasing activity as follows: AT-CuMn-B (202 °C) > AT-CuMn-S (223 °C) ≈ AT-Mn-B (224 °C) > AT-LaMn-P (230 °C). It is evident that Cu promoted MnO_2 catalysts show highly activity for the total oxidation of toluene as compared to the undoped MnO_2 catalysts. The most performant catalyst AT-CuMn-B exhibits T_{10}, T_{50} and T_{90} values at 182, 202 and 222 °C, respectively (Table **4**).

Table 4. Catalytic performances of the acid treated catalyst

	$T_{10}(CO_2)$ /°C	$T_{50}(CO_2)$ /°C	$T_{90}(CO_2)$ /°C
AT-CuMn-S	206	223	232
AT-CuMn-B	182	202	222
AT-Mn-B	191	224	247
AT- LaMn-P	215	230	251

These values are less than those reported recently in toluene oxidation over a non -thermally stabilized γ-MnO_2 resulting from the selective removal of three-dimensional ordered macroporous $LaMnO_3$ perovskite [3]. The improved specific activity reported for AT-CuMn-B can be explained through the synergetic effect between Cu and Mn resulting from Cu-O-Mn interactions as evidenced by ToF-SIMS. This is in accordance with previous work highlighting the beneficial role of highly dispersed Cu-O-Mn species at the surface of the catalyst resulting in improved catalytic performance for toluene combustion [13, 24, 25, 26]. A catalytic test of 9 h duration on stream at 240 °C was performed over the two acid treated Cu-Mn oxides. As shown in Fig. **5**, the AT-CuMn-S catalyst deactivates slightly in the first 30 min to stabilize afterwards with time on stream while no deactivation takes place for AT-CuMn-B. At the end of the test, it is observed a toluene conversion into CO_2 of 71 % and 91 % for AT-CuMn-S and AT-CuMn-B, respectively.

3.8. Effect of acid treatment on structural and catalytic performances

A simple acid treatment (HNO_3 10M at 25 °C) has been successfully developed to obtain copper doped γ/ε-MnO_2-like oxides from two different host Cu-Mn oxides, namely a crystallized $CuMn_2O_4$ and a poorly crystallized birnessite-like MnO_2. Interestingly, the transformation of the partial inverse $CuMn_2O_4$ spinel proceeds through the formation of λ-MnO_2 which is stabilized in acidic medium. λ-MnO_2 is a metastable form of manganese dioxide which retains the cubic spinel structure upon copper removal. Such metastable phase has been previously observed but the best of our knowledge only over normal $LiMn_2O_4$ spinel [1]. Herein, the λ-MnO_2 phase is then transformed into γ-MnO_2 which becomes the prevalent Mn oxide species after calcination. Conversely, the poorly crystallized birnessite-like MnO_2 is readily transformed into ε-MnO_2-like oxide. Irrespective of the acid-treatment the resulting Cu-doped Mn oxides have similar textural properties and good redox properties due to prevalence of Mn^{4+} species. However, it is observed a better reducibility at low temperature for AT-CuMn-B as compared to AT-CuMn-S taking advantage of a copper enrichment allowing an easy reduction of manganese species by hydrogen spill-over. Furthermore, static ToF-SIM has been successively applied to identify unequivocally

the formation of $CuOMn^+$ secondary ions attesting of a close interaction between the dopant and manganese through Mn-O-Cu contribution at the outermost surface of the catalyst. Additionally, a semi-quantitative analysis attests of a higher rate of these interactions for AT-CuMn-B in accordance with a highly dispersed copper throughout the Mn oxide matrix. Consequently, the improvement of toluene oxidation ability for AT-CuMn-B in total toluene oxidation can be explained by a better oxide reducibility and oxygen mobility. Copper doping through asymmetric oxygen vacancy site, namely an oxygen vacancy with an asymmetric coordination of cations [27] facilitates the adsorption and activation of gaseous oxygen and promotes the reactivity of oxygen species in the redox reaction considering a usual MvK mechanism over MnO_2 catalysts. These characteristics explain the better catalytic behavior of doped Cu catalysts as compared to the undoped MnO_2 polymorphs.

4.Conclusion

In summary, we report an easy and attractive method to synthesize new copper doped γ/ε-MnO_2-like oxides from two different host Cu-Mn oxides at room temperature using an HNO_3 10M acid-treatment. The AT-CuMn-B catalyst shows the best activity among the different tested (un)doped MnO_2 polymorphs in toluene oxidation. The numerous Cu-O-Mn interactions at the outmost of the catalyst have been responsible for the enhanced catalytic performance. Copper doping through asymmetric oxygen vacancy site promotes the redox properties, improves the reducibility and oxygen mobility. This novel route to copper doped γ/ε-MnO_2-like oxides, through the extension of the selective dissolution concept applied to binary TM oxides, opens new perspectives in the design of novel MnO_2 based catalysts as possible efficient catalysts in VOC oxidation.

Acknowledgments

This research is supported by a European Program INTERREG V France-Wallonie-Flanders (FEDER) (DepollutAir). The "Fonds Européen de Développement Régional (FEDER)", "CNRS", "Région Nord Pas-de-Calais" and "Ministère de l'Education Nationale de l'Enseignement Supérieur et de la Recherche" are acknowledged for fundings of X-ray diffractometers. Chevreul institute (FR 2638), Ministère de l'Enseignement Supérieur et de la Recherche and Région Hauts-de-France are acknowledged for supporting this work. The authors thank Maya Ibrahim and Shilpa Sonar for the catalytic tests, Martine Trentesaux and Pardis Simon, Olivier Gardoll and Laurence Burylo for their contribution in XPS, H_2-TPR and XRD measurements, respectively.

References

[1] J. C. Hunter, Preparation of a New Crystal Form of Manganese Dioxide: λ-MnO_2, J. Solid State Chem. 39 (1981) 142-147.

[2] W. Si, Y. Wang, Y. Peng and J. Li, Selective Dissolution of A-Site Cations in ABO_3 Perovskites: A New Path to High-Performance Catalysts, Angew. Chem. Int. Ed. 54 (2015) 7954-7957.

[3] W. Si, Y. Wang, Y. Peng, X. Li, K. Li and J. Li, A high-efficiency γ-MnO_2-like catalyst in toluene combustion, Chem. Commun. 51 (2015) 14977-14980.

[4] Y. Dong, J. Zhao, J.-Y. Zhang, Y. Chen, X. Yang, Weina Song, L. Wei, W. Li, Synergy of Mn and Ni enhanced catalytic performance for toluene combustion over Ni-doped α-MnO_2 catalysts, Chem. Eng. J. 388 (2020) 124244.

[5] C. Dong, Z. Qu, X. Jiang, Y. Ren, Tuning oxygen vacancy concentration of MnO_2 through metal doping for improved toluene oxidation, J. Hazard. Mater. 391 (2020) 122181.

[6] R. Kumar and S. Das, Physicochemical and Structural Factors in the Sulfuric Acid Leaching of Nickel- and Copper-Bearing Synthetic Birnessites, Metall. Mater. Trans. B 29 (1998) 527-540.

[7] R. Kumar, Anomalous dependence of leachability on surface area during sulphuric acid leaching of nickel- and copper-doped birnessites, Hydrometallurgy 52 (1999) 71-79.

[8] H. Einaga, A. Kiya, S. Yoshioka, Y. Teraoka, Catalytic properties of copper-manganese mixed oxides prepared by coprecipitation using tetramethylammonium hydroxide, Catal. Sci. Technol. 4 (2014) 3713-3722.

[9] E.C. Njagi, C.-H. Chen, H. Genuino, H.Galindo, H. Huang, S.L. Suib, Total oxidation of CO at ambient temperature using copper manganese oxide catalysts prepared by a redox method, Appl. Catal. B. Environ. 99 (2010) 103-110.

[10] J. Wang, J. Zhu, X. Zhou, Y. Du, W. Huang, J. Liu, W. Zhang, J. Shi and H. Chen, Nanoflower-like weak crystallization manganese oxide for efficient removal of low-concentration NO at room temperature, J. Mater. Chem. A 3 (2015) 7631-7638.

[11] M. Villalobos, B. Toner, J. Bargar and G. Sposito, Characterization of the manganese oxide produced by Pseudomonas putida strain MnB1, Geochim. Cosmochim. Acta 67 (2003) 2649-2662.

[12] S. Grangeon, B. Lanson, N. Miyata, Y. Tani, A. Manceau Structure of nanocrystalline phyllomanganates produced by freshwater fungi, Am. Mineral. 95 (2010) 1608-1616.

[13] Z. Ye, J.-M. Giraudon, N. Nuns, P. Simon, N. De Geyter, R. Morent, J.-F. Lamonier, Influence of the preparation method on the activity of copper-manganese oxides for toluene total oxidation, Appl. Catal. B Environ. 223 (2018) 154-165.

[14] J.-M. Giraudon, A. Elhachami, F. Wyzwalski, S. Siffert, A. Aboukaïs, J.-F. Lamonier, G. Leclercq, Studies of the activation process over Pd perovskite-type oxides used for catalytic oxidation of toluene, Appl. Catal. B Environ. 75 (2007) 157-166.

[15] M.C. Biesinger, B.P. Payne, A.P. Grosvenor, L.W.M. Lau, A.R. Gerson, R.S.C. Smart, Resolving surface chemical states in XPS analysis of first row transition metals, oxides and hydroxides: Cr, Mn, Fe, Co and Ni, Appl. Surf. Sci. 257 (2011) 2717-2730.

[16] V. P. Santos, M. F. R. Pereira, J. J. M. Órfão, J. L. Figueiredo, Synthesis and Characterization of Manganese Oxide Catalysts for the Total Oxidation of Ethyl Acetate, Top.Catal. 52 (2009) 470-481.

[17] H. D. Larcher, P. Courjal, R. H. Urbina, B. Gérand, A. Blyr, A. du Pasquier and J-M. Tarascon, Mechanisms of Phase Transformations, Reactivity, and Effect of Bi Species, J. Electrochem. Soc. 145 (1998) 3392-3400.

[18] C. H. Yoder, E. Bushong, X. Liu, V. Weidner, P. McWilliams, K. Martin, J. Lorgunpai, J. Haller and R. W. Schaeffer, The synthesis and solubility of the copper hydroxyl nitrates: gerhardtite, rouaite and likasite, Mineral. Mag. 74 (2010) 433-440.

[19] A. S. Poyraz, W. Song, D. Kriz, C.-H. Kuo, M.S. Seraji and S. L. Suib, Crystalline Mesoporous $K_{2-x}Mn_8O_{16}$ and ε-MnO_2 by Mild Transformations of Amorphous Mesoporous

Manganese Oxides and Their Enhanced Redox Properties, ACS Appl. Mater. Interfaces 6 (2014) 10986-10991.

[20] C. Julien and M. Massot, Spectroscopic studies of the local structure in positive electrodes for lithium batteries, Phys. Chem. Chem. Phys. 4 (2002) 4226-4235.

[21] L.T. Weng, Advances in the surface characterization of heterogeneous catalysts using ToF-SIMS, Appl. Catal. A Gen. 474 (2014) 203-210.

[22] F. Aubriet, C. Poleunis, P. Bertrand, Investigation of the cluster ion formation process for inorganic compounds in static SIMS, Appl. Sci. Surf. 203 (2003) 114-117.

[23] N. Nuns, J.-M. Giraudon, J.-F. Lamonier, S. Siffert and B. Su, ToF-SIMS studies of the TiO_2-ZrO_2 supported palladium as trace level used in the total oxidation of TCE in humid air, Surf. Interface Anal. 45 (2013) 566-569.

[24] H. Wang, Y. Lu, X. Han, C. Lu, H. Wan, Z. Xu, S. Zen, Enhanced catalytic toluene oxidation by interaction between copper oxide and manganese oxide in Cu-O-Mn/γ-Al_2O_3 catalysts, Appl. Surf. Sci. 420 (2017) 260-266.

[25] X. Lia, L. Wanga, Q. Xiaa, Z. Liub and Z. Li, Catalytic oxidation of toluene over copper and manganese based catalysts: Effect of water vapor, Catal. Comm. 14 (2011) 15-19.

[26] X. Hu, S. Li, Y. Chen, W. Qu, J. Chen, Z. Ma and X. Tang, Single-ion copper doping greatly enhances catalytic activity of manganese oxides via electronic interactions, Chem.Commun. 56 (2020) 904-907.

[27] K. Yu, L.-L. Lou, S. Liu, and W. Zhou, Asymmetric Oxygen Vacancies: the Intrinsic Redox Active Sites in Metal Oxide Catalysts, Adv. Sci. 7 (2020) 1901970.

Captions

Figure 1: X-ray diffraction patterns of the starting CuMn-S, acid treated (a), washed (b) and calcined (c).

Figure 2: X-ray diffraction patterns of the starting CuMn-B, acid treated (a), washed (b) and calcined (c).

Figure 3: ToF-SIMS spectra of CuMn-S and AT-CuMn-S in polarity (+); m/z range: 133.5-137.

Figure 4: (a) Light-off curves for the acid treated catalysts, Toluene = 800 ppm, O_2 = 21 %, N_2 balance, GHSV = 30 L/(g_{cat}.h).

Figure 5: Stability tests performed over the Cu doped MnO_2 catalysts at 240 °C; Toluene = 1000 ppm, O_2 = 21 %, N_2 balance, GHSV = 30 L/(g_{cat}.h).

Fig. 1

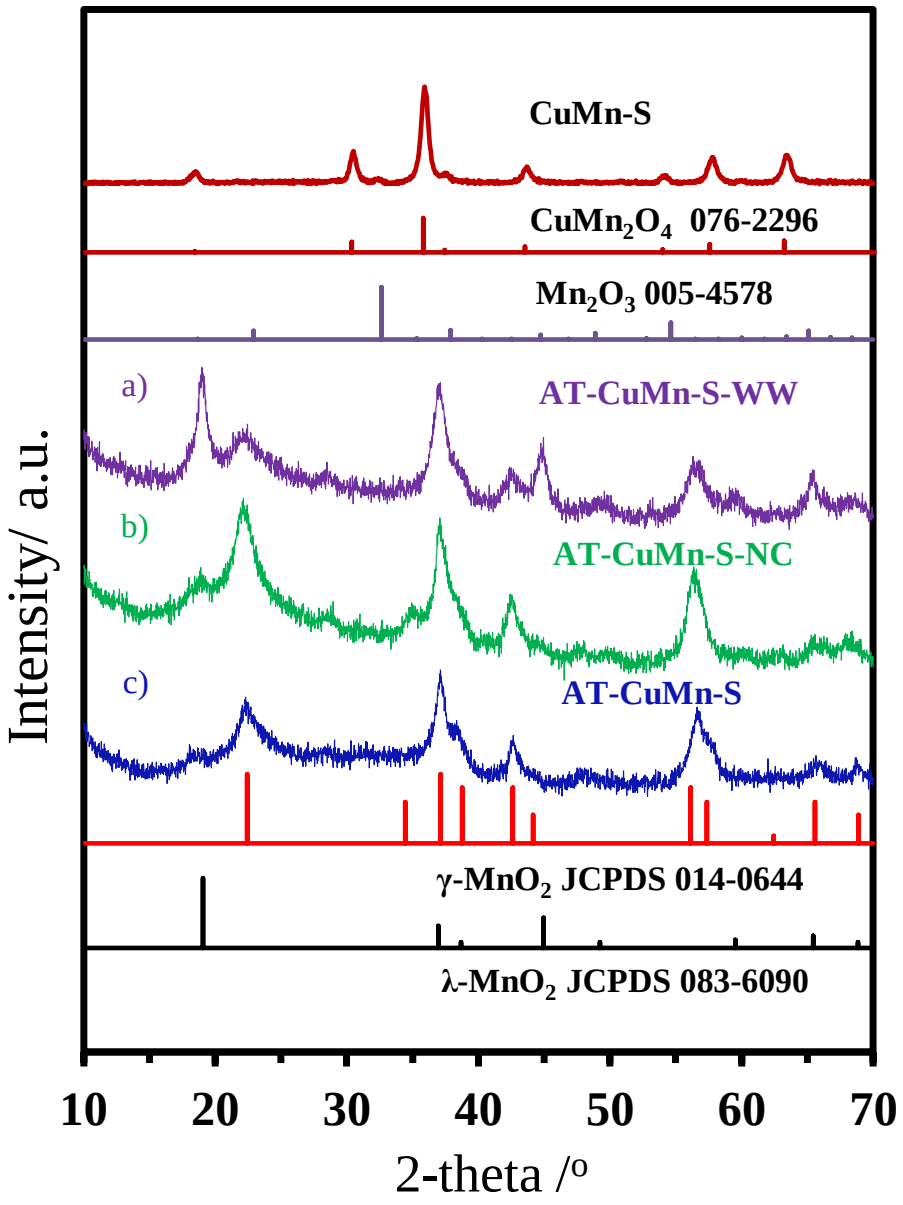
CuMn-S
CuMn2O4 076-2296
Mn2O3 005-4578
a)
AT-CuMn-S-WW
b)
AT-CuMn-S-NC
c)
AT-CuMn-S
γ-MnO2 JCPDS 014-0644
λ-MnO2 JCPDS 083-6090
Intensity/ a.u.
10
20
30
40
50
60
70
2-theta /o

Fig. 2

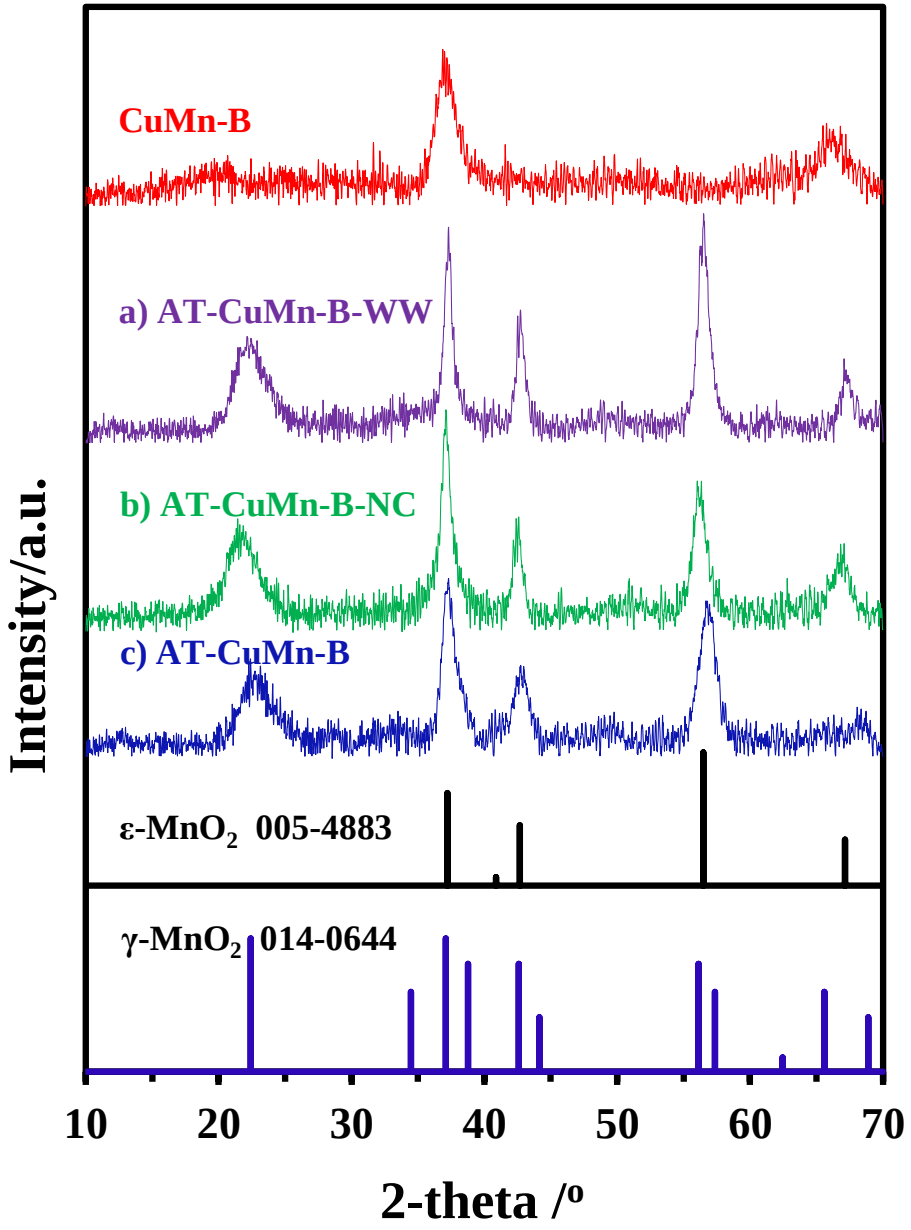
CuMn-B
a) AT-CuMn-B-WW
b) AT-CuMn-B-NC
c) AT-CuMn-B
ε-MnO2 005-4883
γ-MnO2 014-0644
Intensity/a.u.
10
20
30
40
50
60
70
2-theta /o

Fig. 3

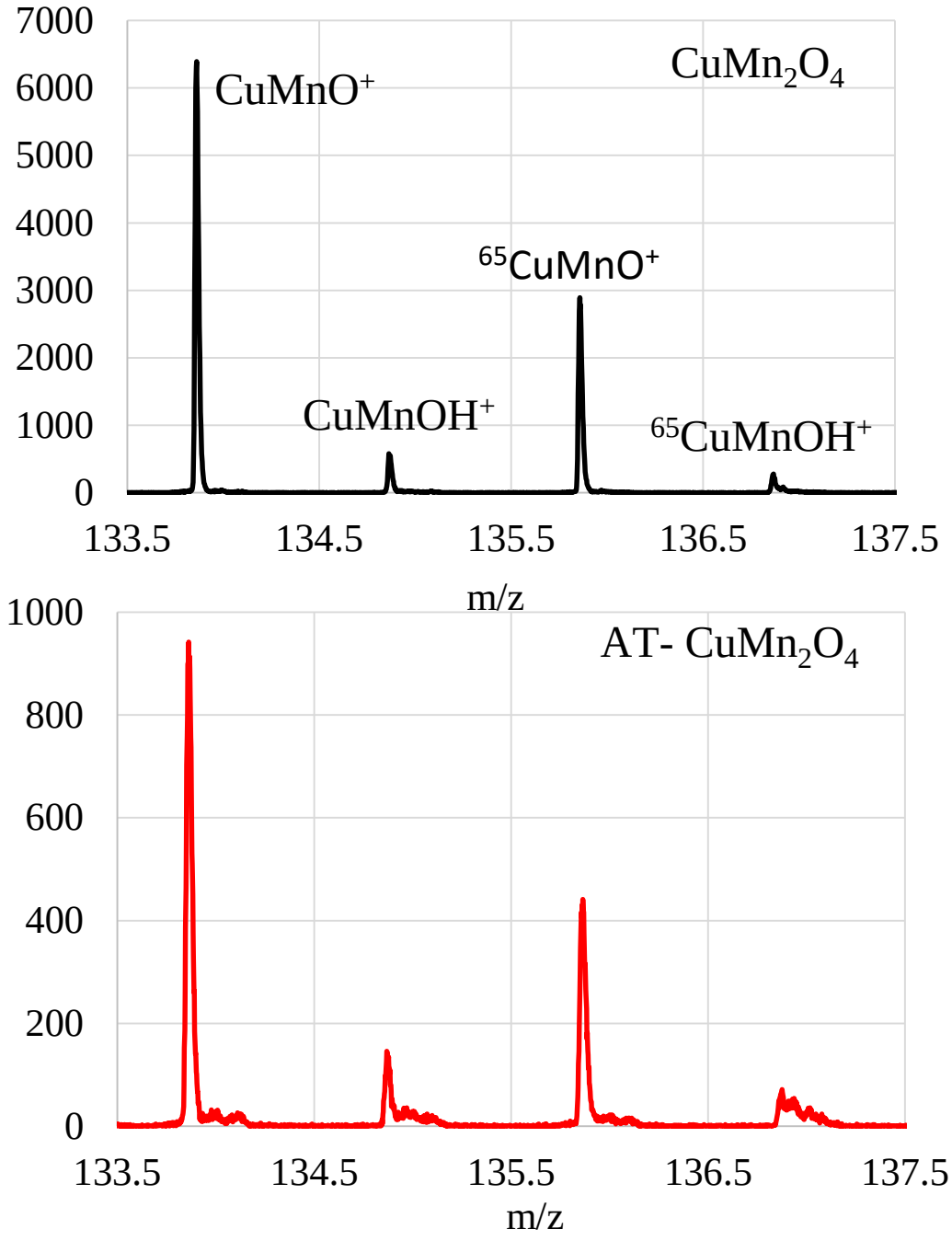
7000
6000
5000
4000
3000
2000
1000
0
CuMnO+
CuMn2O4
65CuMnO+
CuMnOH+
65CuMnOH+
133.5
134.5
135.5
136.5
137.5
m/z
1000
800
600
400
200
0
AT- CuMn2O4
133.5
134.5
135.5
136.5
137.5
m/z

Fig. 4

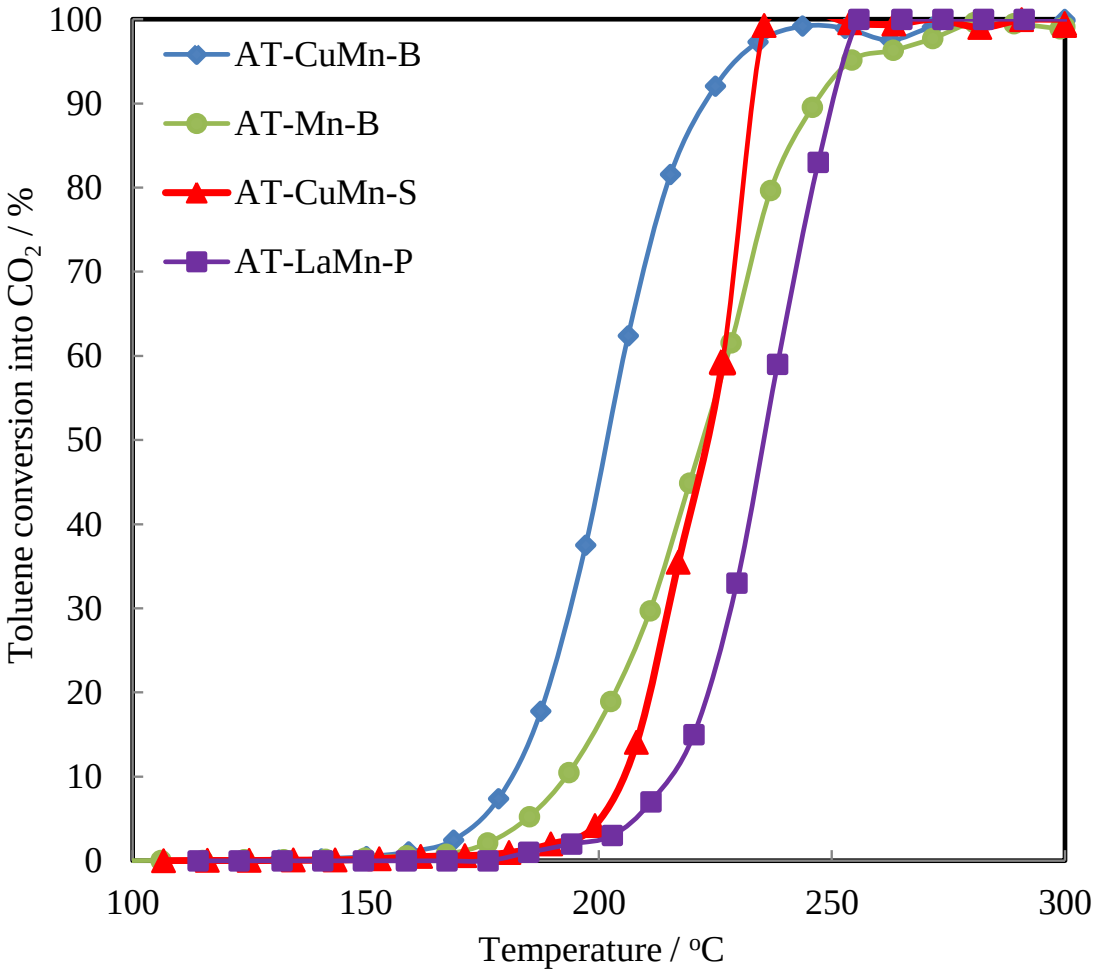
AT-CuMn-B
AT-Mn-B
AT-CuMn-S
AT-LaMn-P
Toluene conversion into CO_2 / %
Temperature / °C
100
90
80
70
60
50
40
30
20
10
0
100
150
200
250
300

Fig. 5

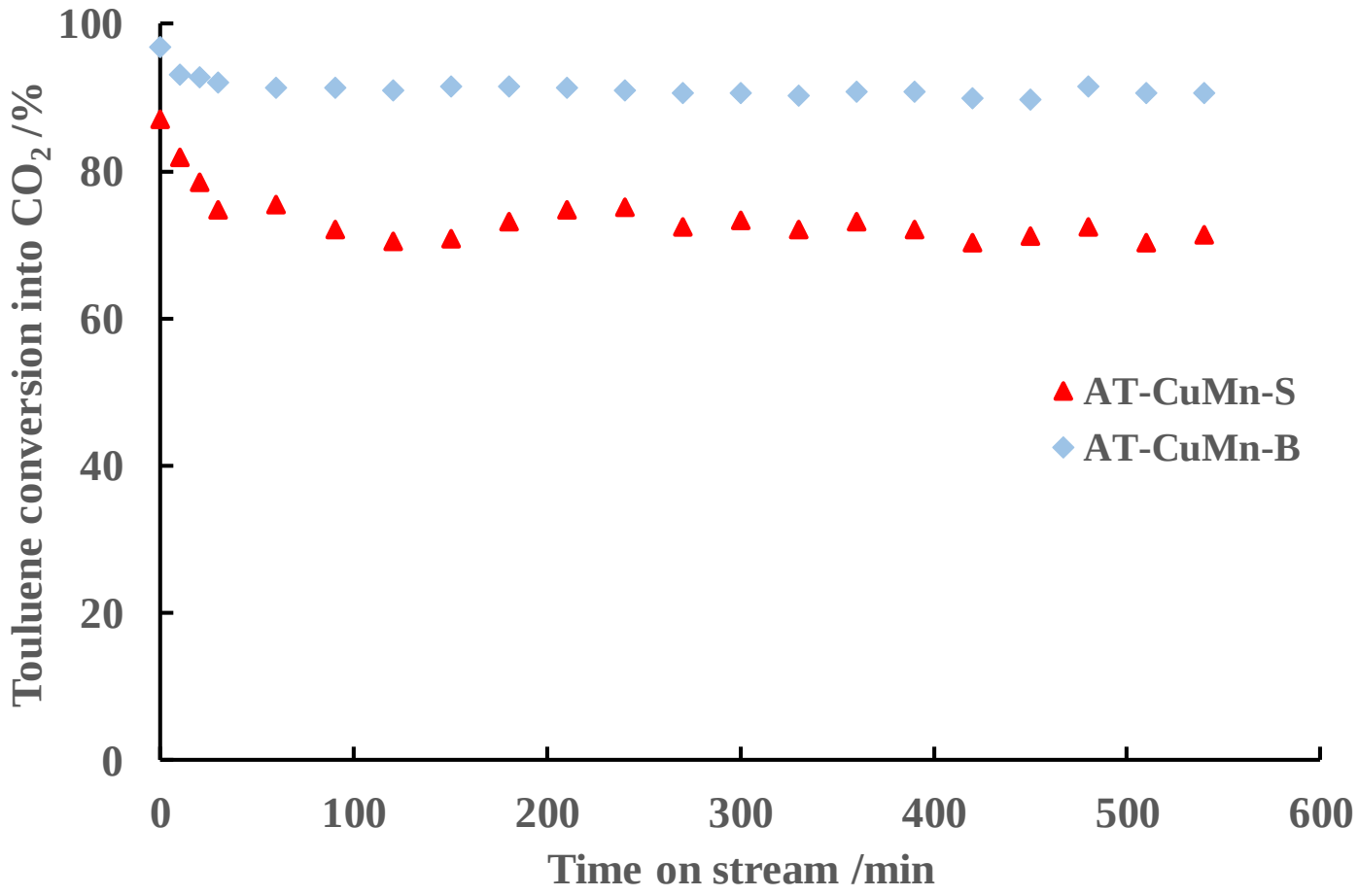
100
80
60
40
20
0
Touluene conversion into CO_2 /%
0
100
200
300
400
500
600
Time on stream /min
AT-CuMn-S
AT-CuMn-B

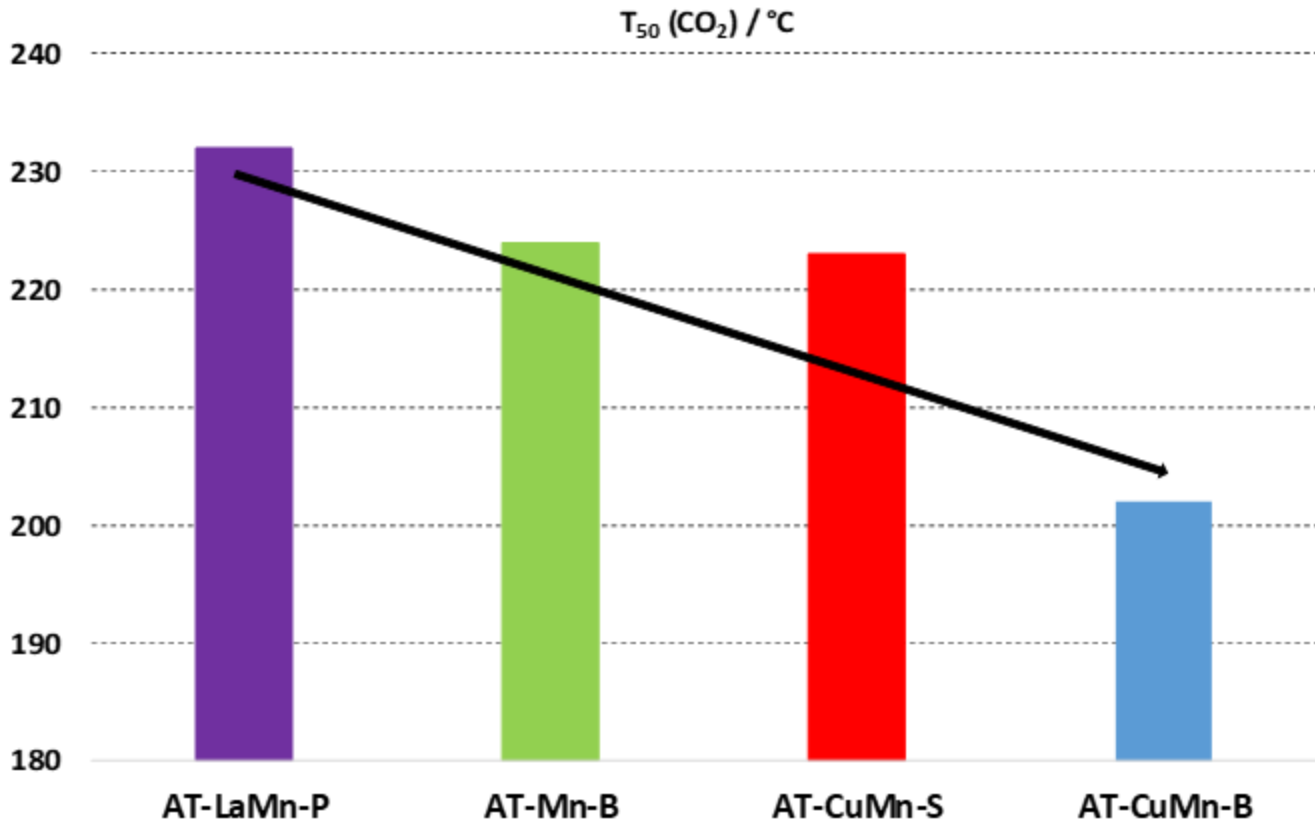

$$C_7H_8 + 9\ O_2 \rightarrow 7\ CO_2 + 4\ H_2O$$